CrossMark

ORIGINAL PAPER

Stress-Induced Permeability Alterations in an Argillaceous Limestone

A. P. S. Selvadurai[1] · A. Głowacki[1]

Abstract The paper presents the results of experiments that were conducted to determine the influence of a triaxial stress state on the evolution of the permeability of an argillaceous limestone. The limestone rock is found in the Ordovician rock formations above the Precambrian basement located in southern Ontario, Canada, which is being considered as a potential host rock for the construction of a deep ground repository for storing low- and intermediate-level nuclear waste. The paper presents the results of an extensive series of hydraulic pulse tests and steady-state tests that were conducted to determine the permeability alterations in zones that can experience levels of damage that can be present in vicinity of an excavated underground opening. A "state-space" relationship is developed to describe permeability evolution with the triaxial stress in the pre-failure regime. The permeability evolution in extensively damaged post-failure states of the rock is also investigated. It is shown that permeability alterations were *four orders of magnitude* higher as a result of significant damage to the material, which is an important consideration in establishing the efficiency of the host rock formation as a barrier for the long-term containment of radionuclide migration.

Keywords Permeability of Cobourg Limestone · Triaxial tests · Obert–Hoek Cell tests · Axial flow pulse tests · Axial flow steady flow tests · Permeability of excavation damage zones

✉ A. P. S. Selvadurai
 patrick.selvadurai@mcgill.ca

[1] Department of Civil Engineering and Applied Mechanics, McGill University, 817 Sherbrooke Street West, Montréal, QC H3A OC3, Canada

1 Introduction

The development of methodologies for the safe geologic disposal of harmful radioactive wastes is an essential requirement for promoting nuclear power generation as a viable approach for mitigating the effects of climate change. Regardless of this perceived benefit, methodologies have to be developed for the disposal of spent fuel and other nuclear wastes that have accumulated through energy production over several decades and the urgency for action is underscored by the fact that the reactor sites themselves, where the hazardous waste is stored temporarily, are reaching their projected service life. Currently, the preferred option for safe disposal of hazardous radioactive material derived from nuclear power generation and other industrial and medical uses is deep geologic disposal and many countries including Argentina, Belgium, Canada, China, Finland, France, Germany, Japan, Russia, Sweden, Spain, Switzerland, UK and the USA have put forward proposals for the development of repositories in geologic formations that are both accessible and considered stable for the active life of the stored hazardous waste. Examples of developments in this area are too numerous to be cited individually, but certain key articles are indicated here to underscore the ongoing efforts in the area of nuclear waste management. The compilation of articles related to safe geologic disposal of nuclear waste given by Laughton et al. (1986) is one of the seminal contributions to the topic. The volumes and articles by Chapman and McKinley (1987), OECD (1988), Selvadurai (1996a, b; 2002), Selvadurai and Nguyen (1997), Huertas et al. (2000), Rutqvist et al. (2005), Selvadurai et al. (2005), Tsang et al. (2008), Pusch et al. (2011), Fraser Harris et al. (2015) and Selvadurai and Suvorov (2016) also provide extensive documentation of the various concepts that have been put

 Springer

forward by the countries mentioned previously, including scoping analyses, in establishing the feasibility of deep geologic disposal concepts for the management of heat-emitting nuclear fuel waste. An extensive evaluation of the Stripa Project of the SKB (the Swedish Nuclear Fuel and Waste Management Company), which was one of the earliest underground research laboratories in a granitic rock that included engineered geologic barriers, is presented by Gray (1993) and Gnirk (1993). Of particular interest to the present research are also the studies by Neuzil (2012) and Neuzil and Provost (2014) which examine the hydromechanical effects that materialize in argillaceous rocks typical of the Cobourg Limestone that has been subjected to effects of glaciation.

The selection and licensing of proposals for deep geologic repository sites is under discussion in many countries. A prelude to the process has been the development of underground research laboratories in geologic settings that closely resemble conditions at potential sites for construction of repositories. The choice of suitable deep geologic repository sites tends to vary with the country, and the choices have ranged from clay deposits in Belgium; granitic rocks in Argentina, Canada, Switzerland, Sweden, Japan and Finland; clay rocks, argillite marls and sedimentary rocks in France, Germany and Switzerland; porous tuffs in the USA and salt formations in Germany and the USA. Recent initiatives in the USA, Russia and Japan have also focused on non-retrievable disposal of high-level nuclear fuel waste in deep boreholes that can extend up the 5 km into the earth's crust either onshore or offshore Selvadurai (2006). In the context of the Canadian nuclear waste management efforts, the emphasis has been on the siting of a deep ground repository in the granitic formations of the Canadian Shield. In recent years, the active attention in other countries on the feasibility of construction of deep ground repositories in argillaceous rock formations, has prompted Canadian agencies to consider the argillaceous limestone in southern Ontario as a possible setting for the construction of a deep geologic repository (DGR) for the disposal of non-heat-emitting low- and intermediate-level nuclear waste. The rationale for the choice of an argillaceous rock formation is the extremely low intact permeability and the potential for accommodating alterations to the stress state in the vicinity of a deep sited underground excavation without severe alterations to the fluid transport properties that can occur in granite formations through the development of major fractures or fissures.

The typical setting of the geologic sequences of the argillaceous rocks of interest to the current research is shown in Fig. 1. Proposals are to construct a DGR in the argillaceous Cobourg (Lindsay) Limestone formation located approximately 600 m below the ground surface. The typical DGR layout can consist of an unsupported excavation that

will serve as the space for the placement of the radioactive waste. The construction of an opening within a geostatically stressed rock mass will lead to stress re-adjustments in the vicinity of the excavation. It is anticipated that the stress re-adjustments will create zones of damage or distress within the rock mass. A recent study was commissioned by the Nuclear Waste Management Organization (NWMO) with regard to the assessment of excavation damaged zones in a repository setting for construction of a repository for low- and intermediate-level nuclear waste. The study by Lanyon (2011) provides a comprehensive account of the underground research laboratories constructed in various countries and focuses on past and present initiatives that attempt to identify *qualitatively*, various levels of mechanical damage that can be induced in the vicinity of the repository setting. Figure 2 illustrates schematically the highly damaged zone (HDZ), the excavation damaged zone (EDZ) and the excavation influenced zone (EIZ) that can be encountered in regions of the host rock close to the DGR opening.

While the qualitative identification of various damaged regions can be straightforward, the geomechanical information necessary to precisely locate the various zones is much more complicated. For example, consider the Zone A (Fig. 2), which corresponds to a HDZ. In order to examine the development of the HDZ, it is necessary to obtain information related to (1) crack initiation, (2) mixed mode crack extension and crack branching and (3) conditions on crack surfaces (open, closed, friction, slip, dilation, degradation, etc.). Ultimately, the primary objective is to establish the evolution of permeability within the HDZ and the quantification of fluid flow characteristics in a highly fractured zone such as a HDZ under generalized stress states. The Zone B in Fig. 2 corresponds to the EDZ, which can be associated with the generation of smaller defects such as microcracks. This is usually described by appeal to continuum damage mechanics, which can, in general, give rise to anisotropic damage mechanics and requires the specification of damage evolution laws. In the practical context of a heterogeneous geologic material such as the Cobourg Limestone, the evolution of damage can also occur in the individual phases (calcite–dolomite-rich nodules and the calcite, dolomite, quartzite containing an argillaceous component) and at the interface between phases. The various damage phenomena can also contribute to anisotropic fluid transport characteristics, the experimental evaluation of which can be extremely complicated. Zone C is classified as the excavation influenced zone where the mechanical and fluid transport characteristics can be identified by properties determined from almost intact samples of the Cobourg Limestone that can be tested in a laboratory environment or from in situ tests. In summary, the permeability characteristics of the Cobourg Limestone will be influenced by the stress state that the rock mass is subjected to during the stress

Fig. 1 Stratigraphy of the rock types that will be encountered in the construction of a deep ground repository in the Ordovician argillaceous limestone, underlain by the Precambrian basement rocks. (*1* Queenston; *2* Georgian Bay; *3* Collingwood; *4* Lindsay; *5* Verulam; *6* Bobcaygeon; *7* Gull River and Shadow Lake; *8* Cambrian Sandstone; *9* Precambrian Basement; *10* Ordovician; *11* Silurian; *12* Devonian; *13* Overburden; *14* Proposed DGR location)
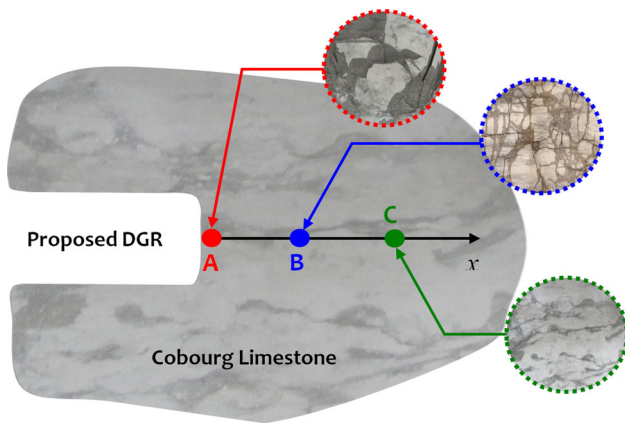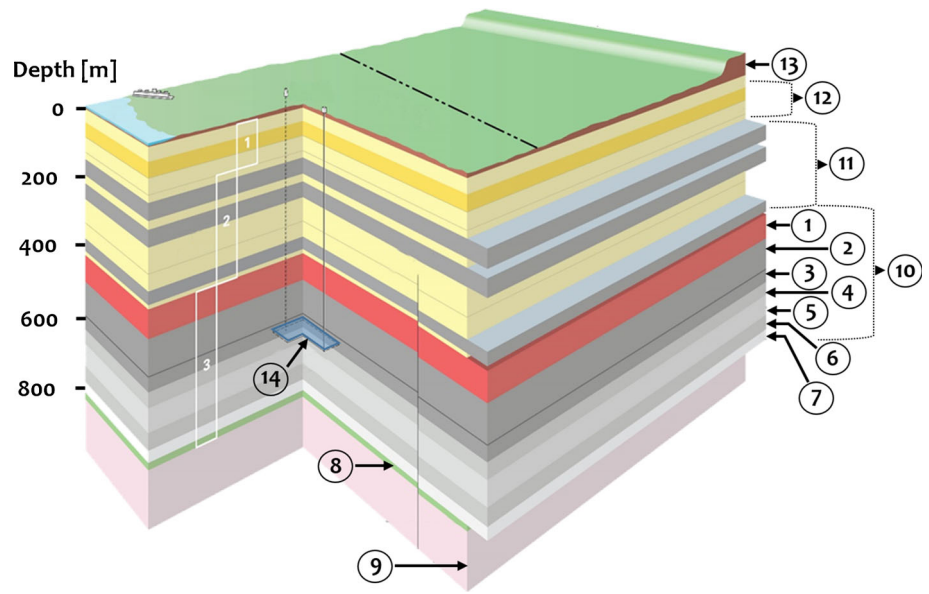

Fig. 2 Schematic view of the damaged regions in the vicinity of a DGR opening

Fig. 3 Results of triaxial tests conducted using the Obert–Hoek Cell—the axis of the test specimen is aligned normal to the nominal plane of the argillaceous partings (Selvadurai 2017)

re-adjustments associated with the construction of a DGR. The mechanistic information available for the description of the stress-affected rock mass is generally not reliable enough to arrive at a complete description of how the permeability evolves with changes in the stress state through purely theoretical considerations. It should also be noted that while permeability can increase in the immediate vicinity of the excavation boundary, an increase in groundwater flow and transport will ultimately be influenced by connected fracture pathways that emanate from the repository (ca. 100's m) to the far field (ca. 1000's m). The role of the EDZ as a potential pathway for the solute and gas migration has also received a great deal of attention (Sykes et al. 2011). The mechanistic influences on the radionuclide migration from a repository setting, however, need further investigation.

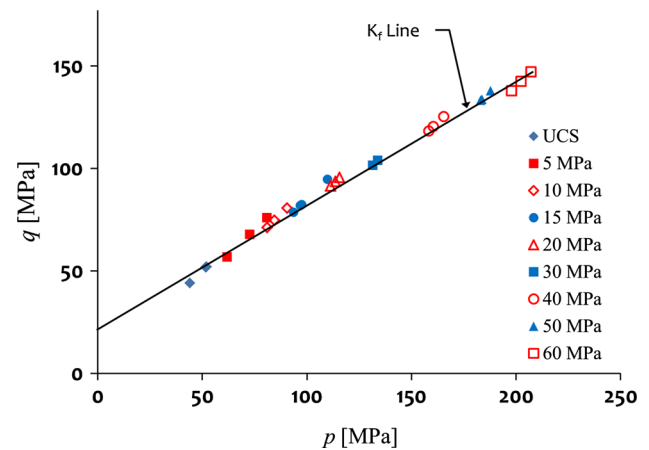In this research, attention is therefore focused on the laboratory investigation of the permeability evolution of the Cobourg Limestone under the action of stress states that can be classified as either in the *sub-failure range* (or the EIZ) and at the *near-failure range* (or the EDZ). In a previous research program (Selvadurai 2017), an extensive set of experiments were conducted to determine the geomechanical properties of the Cobourg Limestone. The Obert–Hoek Test Cell was used to perform experiments on nearly 200 dry samples of the Cobourg Limestone, which were tested to failure. This series of experiments enabled the estimation of the failure envelope for the rock under various states of stresses that could be characterized by the major and minor principal stresses. Figure 3 shows the typical failure envelope for the Cobourg Limestone. The availability of these data has enabled us to embark on a series of tests to investigate the influence of the stress state in the sample, in relation to an excavation influenced

failure stress state (EIZ) or at failure stress states (HDZ to EDZ) on the alteration of permeability. The majority of applications involving the triaxial testing device referred to as the Hoek Cell have focused on its use for the estimation of strength properties of rocks. In this research, the triaxial device (the Obert–Hoek Cell; with due recognition of the contributions of L. Obert) was adapted to measure the permeability characteristics of the argillaceous Cobourg Limestone and its alteration with changes in the triaxial stress state both pre- and post-failure stress states. An exception is the study by Daw (1971) who used the Hoek Cell to conduct steady-state flow tests on intact samples of a coarse-grained rock measuring 25 mm in diameter and 50 mm in length. In that study, no attempts were made to investigate evolution of permeability with stress but the objective was to determine the radial stress necessary to prevent interface leakage between the membrane and rock specimen.

The measurement of the permeability of intact rocks and other geomaterials such as concrete is an extensively researched area of geomechanics and materials engineering. The various laboratory and in situ methods have been proposed for the estimation of permeability of intact and largely unstressed geomaterials such as concrete and rock. Compilations of these studies can be found in the articles by Selvadurai and Carnaffan (1997), Selvadurai and Selvadurai (2010), Selvadurai and Najari (2016) and Pellet and Selvadurai (2016). The research dealing with the influence of external stresses on permeability of rocks is less extensive largely due to the more sophisticated means of applying triaxial stress states to rock samples. Also the investigations should establish the level of the applied stress states in relation to the stress states that can initiate failure in the sample. The path dependency of the application of stresses and the measurement of permeability pre- and post-failure therefore requires extensive experimentation. An early investigation in this area is due to Bernaix (1969) who investigated the permeability of rocks following the failure of the Malpasset Dam in 1959. In this study, steady-state tests are used to measure permeability and the ensuing limitations of establishing steady-state conditions are noted. The work of Brace et al. (1968) represents a seminal study in the area of permeability measurement, where the role of high confining pressures on permeability of Westerly Granite is examined. The work was extended (Brace 1978) to examine permeability evolution with stress in Westerly Granite, Darley Dale Sandstone and Ottawa Sand. Appreciable changes to the permeability evolution have been observed. Other investigations of permeability changes with the stress state are also given by Zoback and Byerlee (1975), Heystee and Roegiers (1980), David et al. (1994), Shiping et al. (1994), Kiyama et al. (1996), Zhu and Wong (1997) and Selvadurai and Głowacki (2008). The recent study by Ding (2013) also addresses the stress-induced permeability evolution aspects with emphasis on use of acoustic emission techniques for the detection of defects. The characteristic features of permeability reduction under isotropic compression and permeability enhancement under deviatoric stresses are indicated in these studies. Heystee and Roegiers (1980) also indicate instances where increases in permeability are observed under the action of tensile stresses. Souley et al. (2001) have used results of tests conducted on the granite from the URL in Pinawa, Canada, to show permeability alterations well below the peak loads. Massart and Selvadurai (2012, 2014) have developed computational approaches for examining permeability evolution at the grain scale. In a majority of these investigations, the rock fabric is homogenous in the grain scale and the permeability alteration is through development of pore closure and pore collapse and microcrack development. Selvadurai (2004) has also implemented the experimental results presented in these studies to develop a damage mechanics-based poromechanical model where the permeability changes are related to damage evolution in the pre-failure stress ranges. The recent study by Wang et al. (2014) deals with the stress-induced alteration of hydromechanical properties of an altered biotite–granite gneiss through development of discrete cracks. The permeability evolution is examined in relation changes in volumetric strain.

In previous research involving the Cobourg Limestone, the intact permeability was determined from one-dimensional steady-state and one-dimensional hydraulic pulse tests on unstressed samples. From a review of these studies (Raven et al. 1992; Vilks and Miller 2007; Gartner Lee Ltd. 2008; Mazurek 2004; Selvadurai et al. 2011, Selvadurai and Jenner 2013; Selvadurai and Najari 2016), the reference permeability of the intact rock is estimated at $K = 1 \times 10^{-20} \, \text{m}^2$. It should also be noted that extensive in situ investigations have been completed to determine the permeability characteristics of the Cobourg and other low-permeability Ordovician rocks (Jensen et al. 2009; INTERA 2011). The in situ state of stress under field conditions is therefore needed to assess the influence of the stress state on permeability values estimated from field tests.

In this research program, triaxial tests were performed on cylindrical samples of the Cobourg Limestone, measuring approximately 85 mm in diameter and either 86 mm and 127 mm in length, under either saturated or unsaturated conditions. One-dimensional permeability experiments are performed, using both steady-state and hydraulic pulse tests to determine the permeability characteristics of the Cobourg Limestone corresponding to stress states that can be identified in relation to the development of failure.

2 Cobourg Limestone Sample Preparation

The term "*undisturbed sample*" is perhaps a misnomer in the context of samples that are used in *any* laboratory investigation or for that matter in a field investigation in a borehole setting. All recovered or fabricated samples will experience some level of disturbance, and this will vary with the sample recovery and fabrication process and the strength characteristics of the rock. Also, the mere action of stress relief associated with sample recovery at depth can introduce sample disturbance and alterations to the geomechanical properties. In this research program, adequate attention is paid to the recovery and fabrication of samples. The Cobourg Limestone samples used in this experimental research were obtained from a block that was recovered from the Saint Mary's Quarry in Bowmanville, Ontario. The block was wet cored, perpendicular to the bedding plane, using a diamond-tipped corer. The cored samples were then lightly machined to the diameter that could be accommodated in the Obert–Hoek Cell. The cylinders were cut to length, and the ends were wet ground to attain parallel end planes that fit properly into the Obert–Hoek Cell. The cylindrical samples in this research measured (85.11 ± 0.49) mm in diameter and (127.30 ± 7.55) mm and (86.02 ± 1.56) mm in length.

Cobourg Limestone has a heterogeneous fabric consisting of nodular limestone regions interspersed with argillaceous partings. The nodular regions predominantly consist of carbonates (84%) calcite and dolomite and quartz (8%) with traces of clays (0.3%). The argillaceous partings contain carbonates (66%) calcite and dolomite, quartz (22%) and a clay content of (2.4%) (illite, kaolinite and a trace of montmorillonite). The porosity (n) of the Cobourg Limestone exhibits variability consistent with heterogeneity of the rock. The porosity obtained from a saturation sequence gave a value of $n = 0.006$, which can be compared with the value of $n = 0.015$ obtained using a vacuum water saturation technique by Selvadurai et al. (2011). The physical and mechanical properties of the Cobourg Limestone obtained from the current experimental program and supplemented by results given by Golder Assoc. (2003), OPG (2011), INTERA (2011), Selvadurai et al. (2011) are as follows: *bulk unit weight*: $\gamma \approx 27$ kN/m³; *porosity*: $n \approx 0.006$; *unconfined compressive strength*: $\sigma_C \approx (113 \pm 25)$ MPa; *tensile strength*: $\sigma_T \approx 6$ MPa; *Young's modulus*: $E \approx 35$ GPa; *Poisson's ratio*: $v \approx 0.25$.

3 Test Facilities and Experimental Procedures

The research presented in this paper was conducted using an Obert–Hoek Triaxial Cell (Obert 1963; Hoek and Franklin 1968), which is capable of testing samples measuring 85 mm in diameter and 170 mm in height. This cell was modified to conduct permeability tests on the rock in a stressed state. A schematic view of the modified Obert–Hoek Cell is shown in Fig. 4. The modifications allowed for better control and application of the axial and radial stresses. The radial stress was applied through the pressurization of the internal rubber (nitrile) membrane. This radial stress was primed by a manual hydraulic pump and maintained by a digitally controlled servo-hydraulic system. The axial stress was applied using stainless steel cylindrical loading platens. Two types of testing machines were used for the application of the axial stresses: When permeability testing was carried out in the pre-failure range, the tests were conducted using the High-Capacity Load Controlled Testing Facility (Fig. 4) where the axial load was controlled using a 65-MPa capacity pressure controller. When permeability testing was carried out at the post-peak or post-failure stress levels, it was necessary to maintain the stresses at a stable level throughout the permeability test and this was accomplished with the servo-controlled rock testing machine (Fig. 5).

The test specimen was placed between upper and lower stainless steel loading platens (Fig. 4). Both platens contained entry ports to provide water inflow and outflow. The interfaces between the plane ends of the platens and the sample were provided with porous stainless steel diffuser disks that distributed the water evenly to the plane end of the cylindrical sample. The rubber membrane (nitrile; thickness 2.4 mm) used to seal the sample was capable of withstanding the applied peak cell pressures, up 60 MPa without rupture when in contact with the smooth cylindrical surface of the Cobourg Limestone sample and the loading platens. The absence of interface leakage was verified by conducting a series of tests where the rock specimen was replaced by an aluminum cylinder with a smooth surface. From previous permeability testing exercises conducted on Indiana Limestone (Selvadurai and Głowacki 2008) and on the Cobourg Limestone (Selvadurai et al. 2011), it was established that a radial stress of 5 MPa was sufficient to provide a complete seal between the rubber (nitrile) membrane and the sample to prevent interface flow during permeability testing. Due to the large radial stresses applied during testing, there was a concern that friction effects could interfere with the accurate measurement of the axial stresses. Separate experiments were conducted to estimate the influence of friction between the membrane and the sample at peak radial stresses of 60 MPa (Selvadurai 2017). It was observed that complete frictional sliding did not occur; the frictional behavior was plastic/elastic with complete recovery of deformations upon release of the axial load. The results obtained indicated that at a radial stress level of 60 MPa, the frictional loss was approximately 2% of the applied axial load and therefore the frictional effects were disregarded in the estimation of the axial stresses to the sample.

Fig. 4 The Obert–Hoek Test Cell and the testing facilities
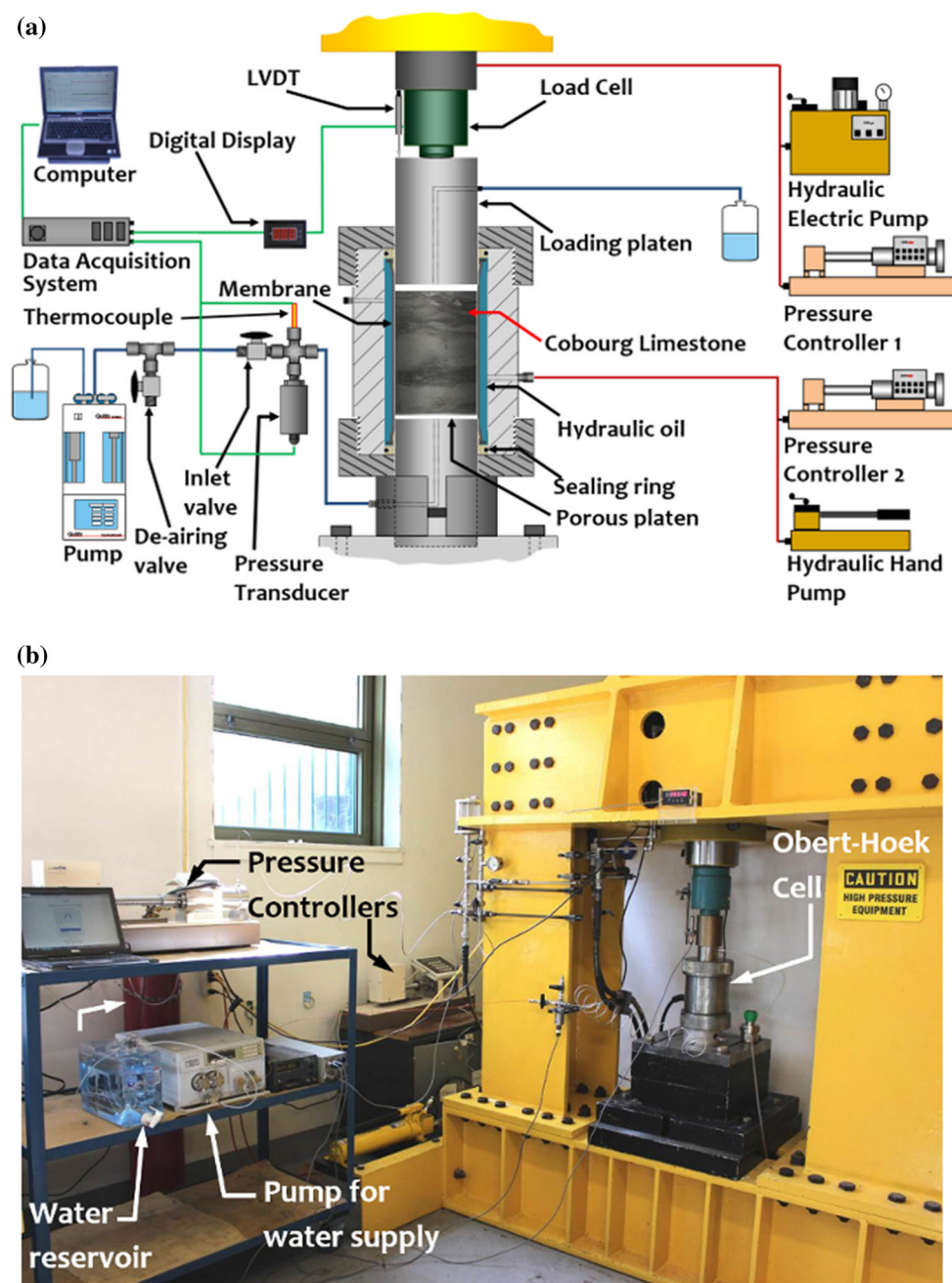
The permeability alterations in the pre-failure regime were determined using hydraulic pulse tests. The fluid supply necessary to initiate the fluid cavity pressurization was supplied at flow rates of 1.0 mL/min using a liquid chromatography pump. When steady-state tests are performed in the post-failure state, a high precision pump was used for the fluid supply. The inlet fluid pressure was monitored using a pressure transducer attached to the water supply line. The radial stress (σ_3), the inlet fluid pressure, the temperature of the permeating water and the axial stress (σ_1), were monitored throughout the tests. All data were saved in a desktop computer using a commercially available data acquisition system.

For the estimation of permeability in the pre-failure stress regime, it was particularly important to ensure that the sample was fully saturated prior to hydraulic pulse testing. With low-permeability materials, pressure artifacts in the form of residual fluid pressures can be present. Selvadurai (2009) examined the influence of residual hydraulic gradients on the response of the 1-D hydraulic pulse tests as well as the degree of saturation on the performance of the axial flow pulse test (Selvadurai and Ichikawa 2013). In this research, the sample was placed in
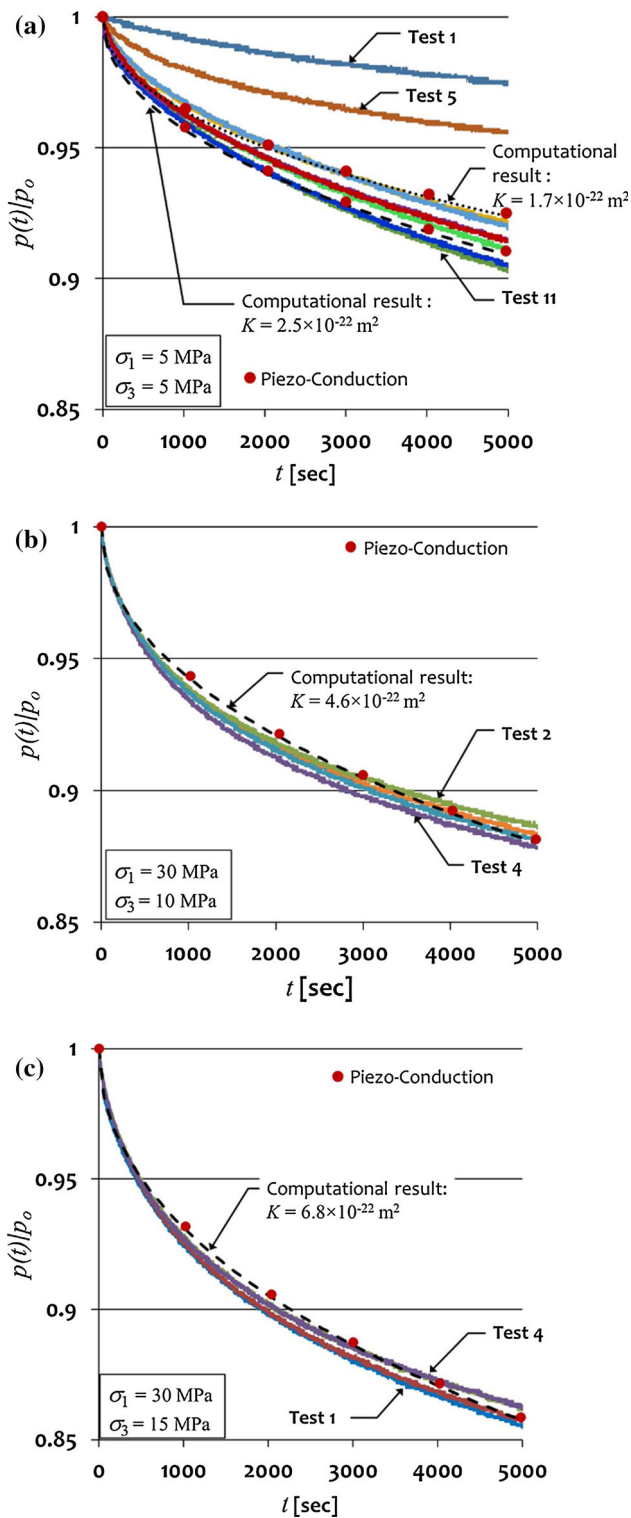
Fig. 5 Typical cavity pressure decay patterns during hydraulic pulse testing of triaxially stressed Cobourg Limestone cylinders: **a** isotropic compression, **b** unloading with $\sigma_1 = $ constant and **c** reloading with $\sigma_1 = $ constant

a vacuum chamber (-78 kPa) for a period of 79 days. The gain in mass was measured until it stabilized with an accuracy of $\pm 0.005\%$ between measurements, at which point the sample was considered to be saturated. The sample was retained in the chamber for a period of 25 days to allow for dissipation of any negative pressures. The temperature of the water used in the permeability experiments was between 23 and 31 °C during the period of testing that lasted over several months (the open conditions in the Structural Engineering Laboratory housing servo-controlled rock testing machine, made it difficult to precisely control the test temperatures). The viscosity of water is altered by changes in temperature, and this is taken into account in the estimation of the permeability. The permeating fluid used throughout the testing was de-aired tap water with a pH of approximately 6.8, measured using a pH analyzer.

4 Permeability Testing of the Cobourg Limestone

4.1 Hydraulic Pulse Testing in the Pre-Failure Stress Range

All stresses applied to the Cobourg Limestone sample are considered to be the total principal stresses, where σ_1 is the total axial stress and σ_3 is the total radial stress. This approximation is justified since the fluid pressures applied to the test specimen during either hydraulic pulse or steady-state tests were, on average, less than 400 kPa. The pressure buildup necessary to conduct the hydraulic pulse tests was provided by supplying de-aired water at a flow rate of 1 mL/min and pressurizing the inflow lines up to 200 kPa. Initially, approximately 475 s was required to pressurize the system up to 200 kPa at a flow rate of 1 mL/min. This time was considered to be excessive since leakage could occur into the rock prior to the start of the pulse test. Therefore, steps were taken to reduce the trapped air in the system, which is known to contribute to slow pressure buildup (Selvadurai and Najari 2015, 2016). The water used in the experiments was distilled and de-aired using a helium gas purging technique. The helium was supplied to the water at flow rate of 10 ml/min at room temperature and a pressure of 250 kPa. The helium was introduced into the water through a diffuser at least 30 min prior to testing, in order to reduce the dissolved air content from 8 to 2 ppm in the 10-liter reservoir. This produces air-deprived water that can flush out pockets of air in the pressurized region in the hydraulic pulse test. Furthermore, the fluid pressure within the fittings, excluding the Obert–Hoek Cell, was

raised to 600 kPa and released in order to flush out trapped air via a de-airing valve. These procedures reduced the pressurizing time from 475 to 180 s. In order to further reduce the pressurizing time, a vacuum venturi (-78 kPa) was attached to the pressurizing lines to de-air the water within the lines and within the pump. A HPLC pump was also air-purged following the manufacturer's recommended procedure, using a syringe to extract any air. Finally, in order to remove air from the Obert–Hoek Cell, the porous disk at the inlet and around the sample–membrane interface, the radial pressure was reduced to 600 kPa and the water inlet end pressurized to 200 kPa. The procedure was stopped when water emerged from around the upper loading platen (Fig. 4a). After performing these de-airing procedures, the time required to pressurize the fluid region in contact with the Cobourg Limestone sample was reduced to 68 s, which was considered acceptable for performing hydraulic pulse tests on the Cobourg Limestone.

In order to dissipate any residual pressures generated during a preceding test, 8 h was allowed to lapse between tests (Selvadurai et al. 2011). The sample was initially subjected to an isotropic stress state of $\sigma_1 = \sigma_3 = 5$ MPa and subjected to a pressure pulse of $p_0 = 200$ kPa. Altogether 16 hydraulic pulse tests were conducted to determine the reference permeability of the Cobourg Limestone. Next, the radial stress and the axial stress were increased incrementally, in stages of 5 MPa, so that the stress state applied to the sample was always maintained isotropic. Hydraulic pulse tests were then conducted on the sample at isotropic stress levels of 15 MPa (11 tests) and 30 MPa (10 tests) Typical results for the pressure decay in the cavity during the hydraulic pulse tests are shown in Fig. 5. The pre-failure permeability testing was extended to include progressive reduction of the radial stress while maintaining the axial stress constant at 30 MPa. This reduction in the radial stress is intended to examine the permeability evolution, for example, during the construction of a *deep ground repository*, when the minor principal stress can be reduced due to construction-related stress relief. The radial stress was first reduced to 25 MPa, and 4 hydraulic pulse tests were conducted to estimate the permeability. The procedure was repeated at the following levels of the minor principal stress: $\sigma_3 = 20$ MPa (6 tests), 15 MPa (6 tests), 10 MPa (4 tests) and 5 MPa (5 tests). Finally, the radial stress was increased, successively, from $\sigma_3 = 5$ MPa to $\sigma_3 = 15$ MPa (4 tests) and then to $\sigma_3 = 30$ MPa (6 tests) while maintaining the axial stress $\sigma_1 = 30$ MPa, in order to establish any evidence of permeability hysteresis during the loading–unloading–reloading cycles. The number of hydraulic pulse tests conducted for each stress state in the pre-failure stress range varied between 4 and 16, depending on the level of repeatability of the pressure decay curves.

Altogether 77 hydraulic pulse tests were performed to estimate the pre-failure stress-induced alterations of permeability of the Cobourg Limestone. After completion of the pre-failure permeability tests, the sample was inspected for damage and for any evidence of permanent alterations in the dimension of the sample. As was observed by Selvadurai et al. (2011), the pre-failure deformations during isotropic compression of the Cobourg Limestone are largely reversible and do not result in observable changes to the dimensions of the sample. Similar conclusions apply when samples are subjected to moderate anisotropic stress fields that were within the failure regime. These stress excursions, however, result in alterations to the permeability of the Cobourg Limestone, and the results will be discussed in a subsequent section.

4.2 Steady-State Permeability Testing in the Post-Failure Range

Prior to conducting the triaxial tests, the system, including the space between the sample and the Obert–Hoek Cell wall, was flooded and all the trapped air was removed. In this series of permeability tests, twelve samples of the Cobourg Limestone were subjected to different radial stress levels (10, 20, 30 MPa) and the axial stress was increased until failure occurred, detected by the attainment of a peak axial stress. In order to accurately maintain the post-failure triaxial stress state, the experiments were performed using the servo-controlled rock testing facility (Fig. 6). Axial flow permeability tests were performed while the sample was in the failed stress state. Initially, the sample was subjected to incremental increases (usually increments of 5 MPa) of the radial and axial stresses until a specific isotropic stress state was attained (i.e., a radial stress $\sigma_3 = 20$ MPa and an axial compressive stress $\sigma_1 = 20$ MPa). At this isotropic stress state, a steady axial
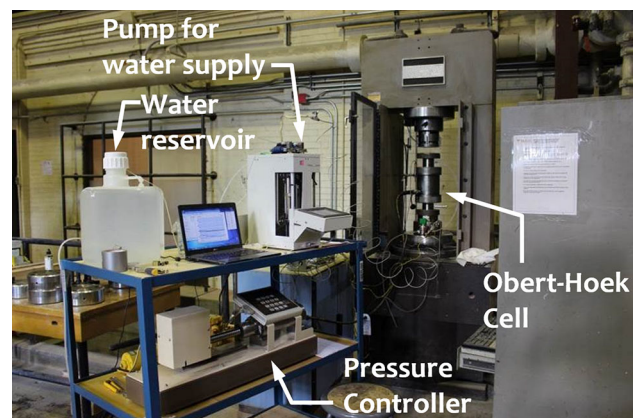

Fig. 6 The servo-controlled rock testing apparatus with the Obert–Hoek Cell setup for post-failure permeability testing

loading was applied to the sample, at a displacement rate of 0.2 mm/min, until failure occurred. During this initial loading to failure, a constant fluid pressure of 100 kPa was applied to the base of the Cobourg Limestone sample using a high precision pump (flow rates accurate to 0.001 mL/min with a volume resolution of 2.5 nL) and the pressure was continuously monitored using the DAQ system. Once the sample failed, the load was allowed to decay/reduce to a stable axial stress state by axial stress cycling: i.e., unloading at a displacement rate of 0.4 mm/min to the initial isotropic stress state and reloading. Typical results for the loading history as represented by the deviator stress $(\sigma_1 - \sigma_3)$ versus axial strain, are shown in Fig. 7. In certain tests post-failure, the pore pressure was allowed to decay and the results were used to estimate the permeability. The stable stress state plateau was maintained for 5 h by pausing the loading rate (i.e., 0 mm/min), using the servo-controlled testing sequences available in the servo-controlled rock testing facility. Some deviator stress reductions did occur (i.e., varying between 10 and 37% of the peak deviator stress), depending on the axial stress level; these results will be presented and discussed in subsequent sections. At the stabilized post-peak stress level, steady flow was initiated from the base of the sample to determine the effective permeability of a Cobourg Limestone sample that has experienced distributed damage and/or failure. Constraints on the access to the servo-controlled rock testing equipment required that the steady-state permeability tests had to be completed within a 5-h period. In general, steady flow through the failed Cobourg Limestone sample was established within the allocated period; the typical time history of the attainment of the steady-state pressure at the base of a sample that has attained a failure load is shown in Fig. 8. For each steady-state post-failure permeability test, the objective was to select an appropriate flow rate, taking into consideration the extent of damage to the sample due to the variations in the minor principal stresses. In this study, the inflow rates were between 0.01 and 0.001 mL/min. As is evident from the typical results for the inlet pressure time histories shown in Fig. 8, the inlet flow rates had to be adjusted to ensure that excessive inlet pressures were not generated. Altogether 12 samples were subjected to failure at three levels radial or minor principal stress (10, 20 and 30 MPa). These confining stress states are representative of the stresses that are expected in the Cobourg formation at the location of the DGR (OPG 2011). Upon completion of the steady-state permeability tests on the failed Cobourg Limestone, the cylindrical samples were carefully extracted from the isolating membrane. In general, the samples could be extracted without disturbance, allowing the preparation of panoramic photographic records of the failure zones and/or
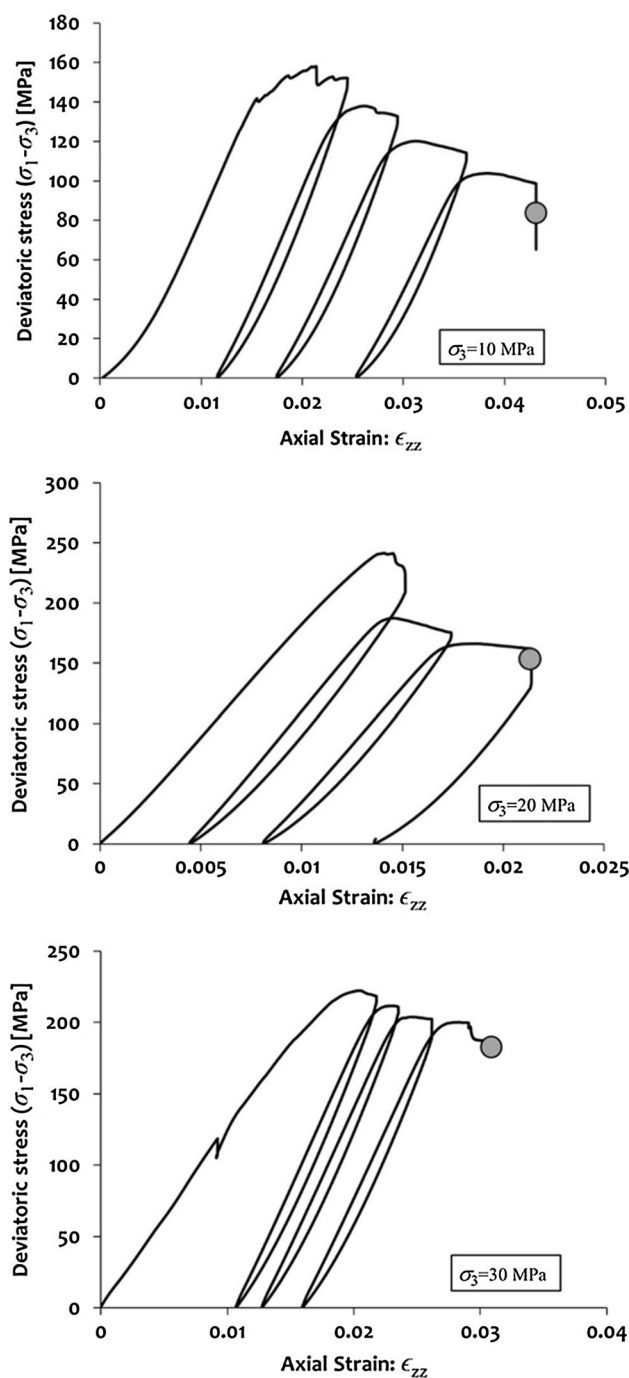

Fig. 7 Typical results for the variation of deviatoric stress applied to the sample with axial strain (*filled circle* indicates the deviatoric stress level at which permeability tests are performed)

failure planes that could have contributed to the alterations in permeability.

Observations of the failure zones and/or planes were enhanced by surface wetting of the sample, providing a useful record of the particular zones through which failure dominates. Figures 9 and 10 illustrate panoramic photographic views of the cylindrical surface of failed Cobourg Limestone
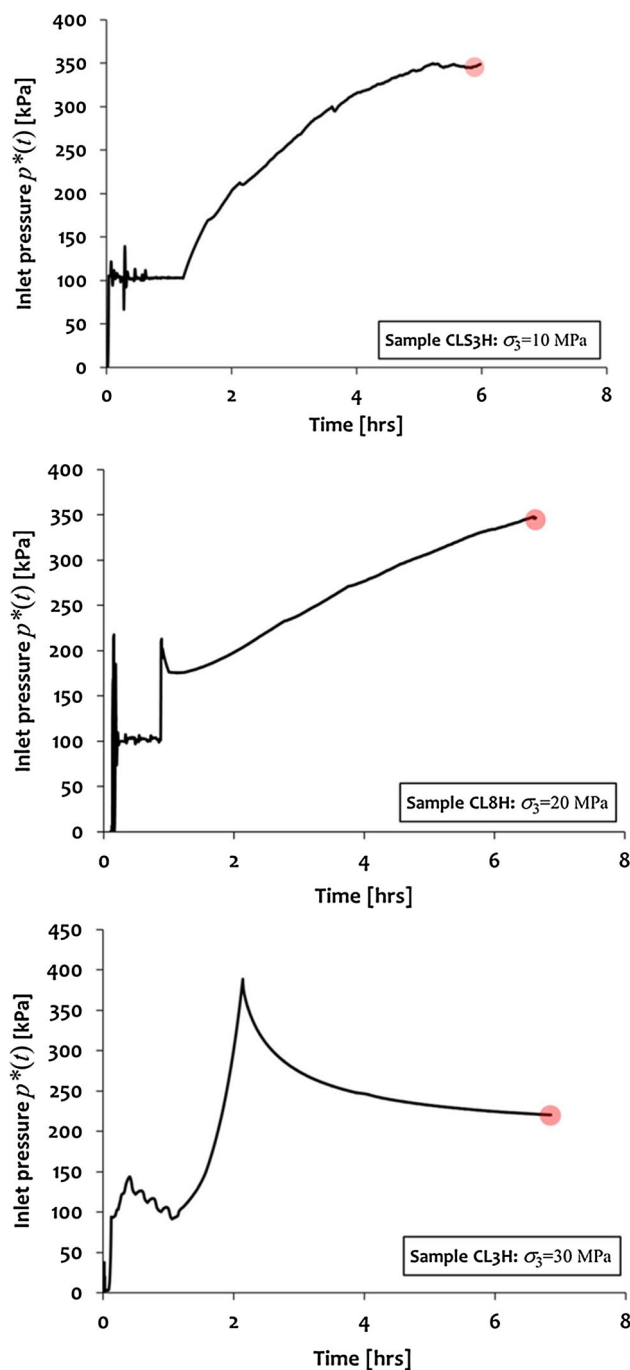
Fig. 8 Time history of the entry point fluid pressure during steady-state permeability tests on failed samples (*filled red circle* indicates the inlet pressure at which steady-state permeability tests are performed) (colour figure online)

samples; a red overlay is used to highlight crack patterns, and the notation refers to the following: K_{SS} is the steady-state permeability, and K_{PD} is the pulse decay permeability. The extent of migration of fluids within the fractures was further confirmed by injecting a red dye tracer into the fractured sample. In these tests, the radial stress was varied and the deviator stress at failure is indicated in Figs. 9 and 10.

5 Theoretical Developments

5.1 Transient Tests in the Pre-Failure Stress Range

The permeability of the Cobourg Limestone investigated in this research assumes that the fluid flow through the rock can be described by an isotropic homogeneous form of Darcy's law (Bear 1972; Selvadurai 2000). This is an idealization since the Cobourg Limestone exhibits heterogeneity and stratifications that can introduce anisotropy. The measure of isotropic permeability is therefore a useful *first approximation* for the description of permeability characteristics of the heterogeneous Cobourg Limestone. The mapping of hydraulic heterogeneity is non-routine (Selvadurai and Selvadurai 2010), and in the present context, the application of stress states to the samples undergoing permeability testing can complicate the interpretation of experimental results. If both datum and velocity heads are neglected in relation to the pressure head, the Bernoulli potential can be expressed in terms of the fluid pressures $p(\mathbf{x})$ (dimensions M/LT^2) and Darcy's law can be written as:

$$\mathbf{v}(\mathbf{x}) = -\frac{K}{\mu}\nabla p(\mathbf{x}) \qquad (1)$$

where $v(x)$ is the velocity vector (L/T) or specific discharge (Darcy's velocity), K is the permeability (L^2), μ is the dynamic viscosity of water (M/TL), ∇ is the gradient operator, and x is a position vector.
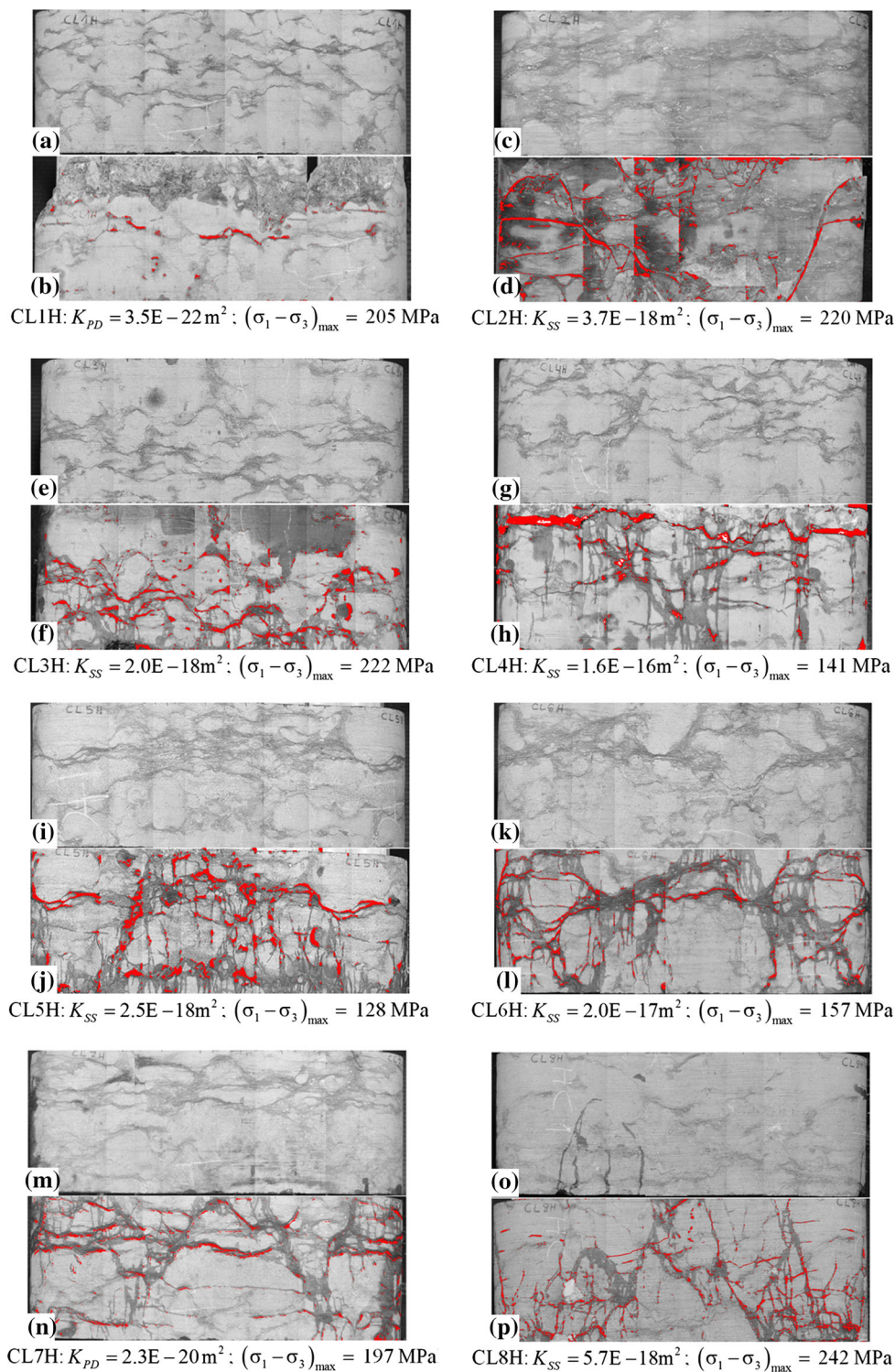
In low-permeability rocks, the most widely accepted method for determining the permeability is based on the hydraulic pulse technique, where a fluid cavity in contact with the saturated porous medium is subjected to a pressure rise and the decay pattern is used to estimate the permeability of the rock. The method is attributed to Brace et al. (1968), and extensive references to further developments, both theoretical and experimental, are given by Selvadurai and Carnaffan (1997) and Selvadurai et al. (2005). The basic approach adopted in the hydraulic pulse testing assumes that the fluid pressures are linked to the deformations of the fluid, the deformations of the porous skeleton and the deformations of the grains composing the porous fabric. The partial differential equation governing the dissipation of fluid pressure in the fluid-saturated porous medium is given by the "piezo-conduction" equation

$$\frac{K}{\mu}\nabla^2 p = S\frac{\partial p}{\partial t} \qquad (2)$$

where S is the storage coefficient, which can be expressed in the form

$$S = nC_w + C_{eff} - (n+1)C_s \qquad (3)$$

Fig. 9 Panoramic views of failure patterns observed on the cylindrical surface of the Cobourg Limestone samples measuring ∼85 mm diameter and ∼120 to 132 mm long (K_{SS} and K_{PD} are permeabilities measured in steady-state and pulse tests. The panoramic view of the intact sample is shown for purposes of comparison)

(a)

(b)

CL1H: $K_{PD} = 3.5\text{E} - 22\,\text{m}^2 : (\sigma_1 - \sigma_3)_{max} = 205$ MPa

(c)

(d)

CL2H: $K_{SS} = 3.7\text{E} - 18\,\text{m}^2 : (\sigma_1 - \sigma_3)_{max} = 220$ MPa

(e)

(f)

CL3H: $K_{SS} = 2.0\text{E} - 18\,\text{m}^2 : (\sigma_1 - \sigma_3)_{max} = 222$ MPa

(g)

(h)

CL4H: $K_{SS} = 1.6\text{E} - 16\,\text{m}^2 : (\sigma_1 - \sigma_3)_{max} = 141$ MPa

(i)

(j)

CL5H: $K_{SS} = 2.5\text{E} - 18\,\text{m}^2 : (\sigma_1 - \sigma_3)_{max} = 128$ MPa

(k)

(l)

CL6H: $K_{SS} = 2.0\text{E} - 17\,\text{m}^2 : (\sigma_1 - \sigma_3)_{max} = 157$ MPa

(m)

(n)

CL7H: $K_{PD} = 2.3\text{E} - 20\,\text{m}^2 : (\sigma_1 - \sigma_3)_{max} = 197$ MPa

(o)

(p)

CL8H: $K_{SS} = 5.7\text{E} - 18\,\text{m}^2 : (\sigma_1 - \sigma_3)_{max} = 242$ MPa

In (3), C_{eff} is the compressibility of the porous skeleton (LT^2/M) and is the inverse of the bulk modulus K_{eff}; C_s is the compressibility of the solid grains, C_w is the compressibility of the pore fluid, and n is the porosity of the medium. In the case of the Cobourg Limestone, mineral heterogeneity makes the measurement of the skeletal compressibility a challenging exercise (i.e., the mineral fractions, their compressibilities and their spatial distributions need to be determined accurately). References to these approaches are numerous, and developments are summarized, among others, by Coussy (2004), Gueguen and Bouteca (2004), Suvorov and Selvadurai (2010),
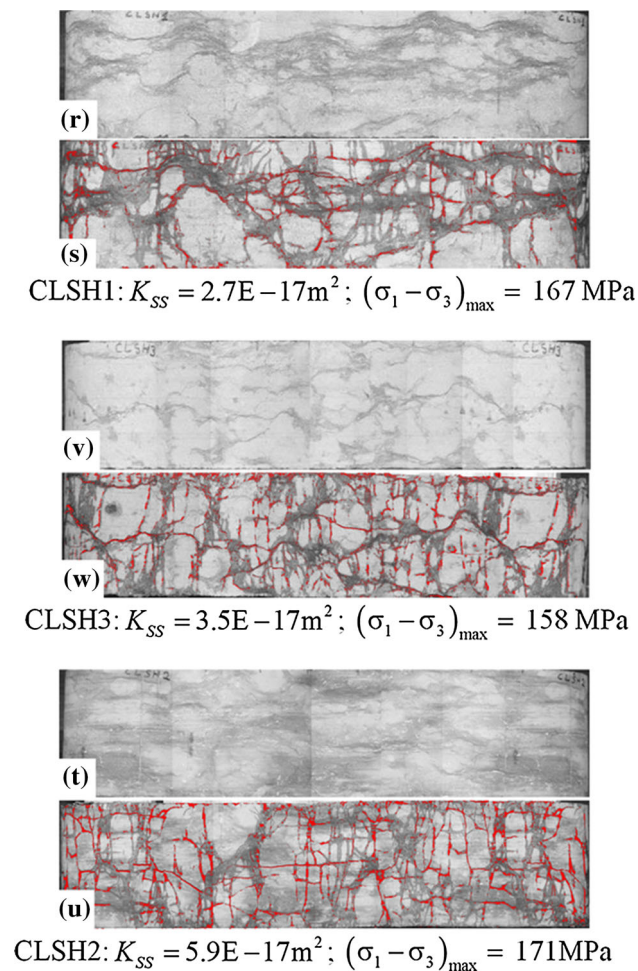
CLSH1: $K_{SS} = 2.7\mathrm{E}-17\,\mathrm{m}^2$; $(\sigma_1 - \sigma_3)_{max} = 167\,\mathrm{MPa}$

CLSH3: $K_{SS} = 3.5\mathrm{E}-17\,\mathrm{m}^2$; $(\sigma_1 - \sigma_3)_{max} = 158\,\mathrm{MPa}$

CLSH2: $K_{SS} = 5.9\mathrm{E}-17\,\mathrm{m}^2$; $(\sigma_1 - \sigma_3)_{max} = 171\,\mathrm{MPa}$

Fig. 10 Panoramic views of failure patterns observed on the cylindrical surface of the Cobourg Limestone samples measuring ∼85 mm diameter and ∼83 to 86 mm long (K_{SS} is the permeability measured in the steady-state test. The panoramic view of the intact sample is shown for purposes of comparison)

Schutjens and Heidug (2012), Cheng (2016), Muller and Sahay (2016) and Selvadurai and Suvorov (2016). An alternative is to use the Biot coefficient α to estimate the compressibility of the porous skeleton, and the relationship for the Biot coefficient is given by:

$$\alpha = \left(1 - \frac{C_s}{C_{\mathrm{eff}}}\right) \tag{4}$$

Ideally, the conditions associated with the hydraulic pulse testing should be examined by appeal to a theory of poroelasticity similar to that proposed by Biot (1941). In the case of one-dimensional hydraulic pulse tests, it has been shown (Hart and Wang 1998; Selvadurai and Najari 2013) that the results obtained from the analysis based on the solution of the piezo-conduction Eq. (3) when incorporating the compressibility of solid grains of the porous medium, are comparable to the complete poroelasticity analysis of the problem. The piezo-conduction equation,

however, is much simpler to implement, and with certain one-dimensional experimental configurations, exact solutions can be developed for time-dependent pressure decay in the pressurized cavity. Also, in a relative sense, as the permeability of a geomaterial increases (e.g., permeability of Indiana Limestone compared to that of Stanstead Granite), the discrepancy between the two set of results (piezo-conduction compared to a Biot poroelasticity analysis) for the time-dependent cavity pressure decay is marginal. In the case of very low-permeability materials, other factors, including residual pressures in the test specimen following a saturation sequence and air voids in the fluid-filled cavity, can also influence the outcome of hydraulic pulse testing (Selvadurai 2009; Selvadurai and Ichikawa 2013; Selvadurai and Najari 2013). In the experimental configurations associated with the hydraulic pulse tests conducted on the Cobourg Limestone, the impervious boundary conditions imposed on the cylindrical surface of the sample render the problem one-dimensional and the governing partial differential Eq. (2) reduces to

$$\frac{K}{\mu}\frac{\partial^2 p}{\partial z^2} = S\frac{\partial p}{\partial t} \tag{5}$$

where z is the axial coordinate. The boundary conditions applicable to the modeling of the one-dimensional piezo-conduction equation are

$$p(0,t) = \tilde{p}(t); \quad \tilde{p}(0) = p_0; \quad \forall t > 0 \tag{6}$$

$$p(L,t) = 0; \quad \forall t \geq 0 \tag{7}$$

where L is the length of the cylinder and the fluid flow-mass conservation compatibility condition imposed at the pressurized boundary takes the form

$$\Phi\left(\frac{\partial p}{\partial z}\right)_{z=0} = \left(\frac{\partial p}{\partial t}\right)_{z=0}; \quad \forall t > 0 \tag{8}$$

In (8)

$$\Phi = \left(\frac{AK}{\mu V_w C_w}\right) \tag{9}$$

and V_w is the volume of the fluid in the pressurized cavity. The initial condition applicable to the hydraulic pulse test is

$$p(z,0) = 0; \quad 0 \leq z \leq L \tag{10}$$

The general solution to this initial boundary value problem applicable to a one-dimensional domain of finite extent has been examined in the literature (Hsieh et al. 1981). For very low-permeability rocks, the analytical solution can be obtained in a compact form by assuming that the domain is of infinite extent. In this case, the pressure decay in the cavity can be expressed as

$$\frac{\tilde{p}(t)}{p_0} = \exp(\Omega^2 t)\text{Erfc}\left(\sqrt{\Omega^2 t}\right) \qquad (11)$$

where

$$\Omega = \Phi\omega; \quad \omega^2 = \frac{S\mu}{K} \qquad (12)$$

and $\text{Erfc}\left(\sqrt{\Omega^2 t}\right)$ is the complementary error function.

An alternative approach to the analysis of the hydraulic pulse test, particularly for a cylinder of finite length, is to seek a computational formulation of the problem using a finite element modeling of the initial boundary value problem described by (5) to (10). The details of the approach are summarized by Selvadurai and Selvadurai (2014) and Selvadurai and Najari (2013, 2015). The finite element model and the mesh refinement necessary to perform the analysis using a computational code that can examine multi-physics processes, are shown in Fig. 11. Selvadurai and Selvadurai (2014) showed that the interface between the fluid-saturated porous medium and the fluid-filled cavity needs adequate mesh refinement to eliminate numerical errors. The procedure for estimating the permeability of the Cobourg Limestone from the results of the cavity pressure decay tests involves varying the permeability input to either the analytical result, Eq. (11) or the computational procedure based on the finite element approach until the decay curves match within the time range of the observations. An exact match is generally not feasible; Selvadurai and Carnaffan (1997) and Selvadurai et al. (2005) advocate assigning bounds to the estimation of permeability. Both the analytical procedure and the computational approach were applied to estimate the performance of the hydraulic pulse tests conducted on the Cobourg Limestone sample subjected to stress histories within the pre-failure stress range. The material parameters used in the modeling exercises were as follows: the skeletal Young's modulus $E = 35$ (GPa); the skeletal Poisson's ratio $v = 0.25$; the Biot coefficient $\alpha = 0.7$; porosity $n = 0.01$; dynamic viscosity of water as $\mu = 0.001$ (Pa s) at 20 °C; density of water $\gamma_w = 998$ (kg/m^3); compressibility of water $C_w = 4.35E-10$ (Pa^{-1}); volume of the pressurized fluid $V_w = 3.67E-5$ m^3; and compressibility of the porous skeleton $C_{eff} = 4.28E-11$ Pa^{-1}. The cavity pressure decay estimates obtained from the two approaches are indicated in the typical pressure decay curves shown in Fig. 5; it is evident that similar results are obtained. The analytical and computational procedures provided a cross-check on the estimates for the permeability of the Cobourg Limestone during the application of stresses in the pre-failure stress range. The results can be presented in several ways, and a convenient representation is to illustrate the evolution of permeability in relation to the combination of the principal stresses σ_1 and σ_3 applied to the test

specimen. Figure 12 presents the normalized permeability evolution pattern with the variations in the stress state. In these series of pre-failure stress state permeability evaluations, the development of an analytical result to describe the variation of permeability with principal stresses σ_1 and σ_3 is meaningful only in the loading stage. The results can be presented in several ways, but a convenient representation is to illustrate the evolution of permeability in relation to the combination of the principal stresses σ_1 and σ_3 applied to the test specimen. Also, since the permeability was evaluated during the application of isotropic stress states, the variation of permeability in the loading path can be expressed as a function of the mean of the applied stresses; i.e., $\sigma_m = (\sigma_1 + 2\sigma_3)/3$. Figure 13 illustrates the variation of permeability with the mean stress during the loading path, and an approximate empirical relationship can be developed in the form

$$\frac{K(\sigma_1,\sigma_3)}{K_0} = \exp\left(\lambda_1^m \frac{\sigma_1}{\sigma_0}\right)\exp\left(\lambda_3^m \frac{\sigma_3}{\sigma_0}\right) \qquad (13)$$

where $\lambda_1^m \simeq 0.28$; $\lambda_3^m \simeq 0.03$, $K_0 = 10^{-22}$ m^2 is the reference permeability, and $\sigma_0 = 5$ MPa is the initial isotropic stress state applied to the Cobourg Limestone. The relationship (13) has a coefficient of determination of 0.84. The development of a similar relationship for the evolution of permeability during a *reduction* in the minor principal stress σ_3 is not feasible since the unloading experiments were conducted at only at a specific value of the major principal stress σ_1. An approximate relationship can, however, be developed by constructing a state-space surface between the isotropic loading path and the unloading path at a constant value of $\sigma_1 = 30$ MPa. The corresponding approximate state-space relationship for unloading can be developed in the form

$$\frac{K(\sigma_1,\sigma_3)}{K_0} = \exp\left(\lambda_1^u \frac{\sigma_1}{\sigma_0}\right) + \exp\left(\lambda_3^u \frac{\sigma_3}{\sigma_0}\right) + \lambda_0^u \qquad (14)$$

where $\lambda_0^u \simeq -1$; $\lambda_1^u \simeq 0.25$; $\lambda_3^u \simeq 0.20$. Figure 14 illustrates the state-space representation corresponding to (14).

5.2 Steady-State Testing in the Post-Failure Stress Range

In the post-failure state, the sample experiences fracturing with no pre-determined orientation of the fracturing planes. This is in contrast to the development of a single fracture in a rock sample; in this case, the fluid transport response has been extensively studied in the geosciences and rock mechanics literature. The conventional parallel plate model can be used to estimate the aperture-dependent evolution of permeability with axial stress. Extensive accounts of developments are given by Nguyen and Selvadurai (1998),

Fig. 11 Computational
modeling of the piezo-
conduction analysis of the
transient permeability test
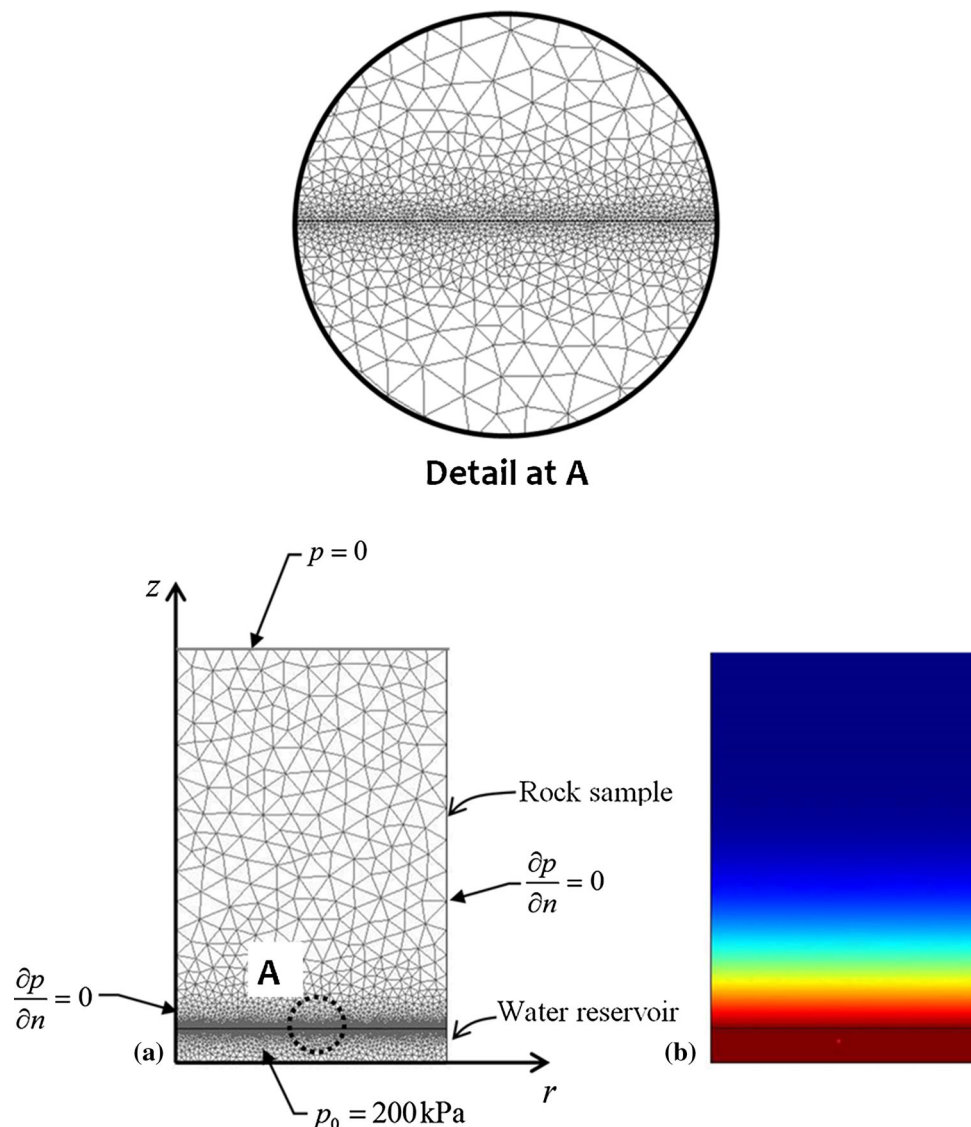
Tao et al. (2011), Selvadurai (2015), Wong et al. (2013),
Wang et al. (2014), Ma and Wang (2016), Han et al.
(2016), Liu et al. (2016), Pellet and Selvadurai (2016) and
in the volume by Gleeson and Ingebritsen (2016). In the
extensively fragmented state, the effective permeability of
the failed Cobourg Limestone can only be interpreted as a
bulk permeability change (i.e., based on the original initial
dimensions of the sample) as interpreted through the
attainment of a steady flow rate over a prescribed hydraulic
gradient. Further refinement of the modeling is merited
only if the exact pathways of fluid transport and the evo-
lution of apertures during application of triaxial stress
states can be mapped by appeal to refined experimentation.
Such facilities and approaches are certainly non-routine
and beyond the scope of the current research program. In
this research, the permeability of an extensively fractured
Cobourg Limestone sample was determined by performing

conventional one-dimensional steady-state permeability
tests. This approach provides only an effective measure of
the permeability of the rock in the axial direction of the
Cobourg Limestone sample with the nominal planes of
stratification normal to the axis of the cylinder. The per-
meability is estimated from the relationship

$$K = \frac{\mu Q L}{A(p_i - p_o)} \tag{15}$$

where p_i and p_o are, respectively, the inlet and outlet
pressures initiating the steady flow rate Q, L is the axial
length of the sample, and A is the gross cross-sectional area
of the sample. The use of the gross cross-sectional area of
the cylindrical sample provides a *lower bound* for the
permeability since the actual cross-sectional area of the
flow path is likely to be lower than the gross cross-sectional
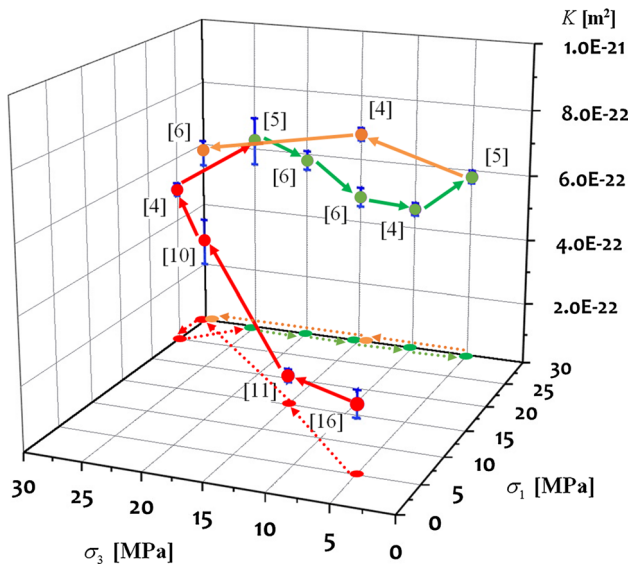area. The permeability of the extensively damaged

Fig. 12 The evolution of permeability of the Cobourg Limestone in the pre-failure stress state
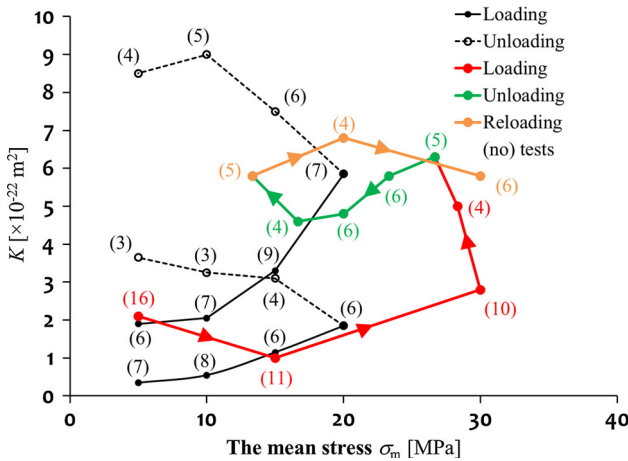

Fig. 13 Permeability evolution of the Cobourg Limestone in pre-failure stress states as a function of the mean stress $\sigma_m = (\sigma_1 + 2\sigma_3)/3$ (the solid and dotted black lines refer to the results obtained by Selvadurai et al. (2011))

Fig. 14 Estimates for the permeability evolution during stress release

Fig. 15 The post-failure permeability of the Cobourg Limestone

deep geologic repository. The creation of a repository in a stressed geologic formation will lead to different levels of damage that can result in the generation of discrete fractures and distributed damage that can have a significant influence on the resulting permeability. Past investigations of the Cobourg Limestone have largely focused on estimating the intact permeability in a *nearly undamaged state*. This is based on the assumption that defects will not develop during sample recovery and preparation for permeability testing. The rock has sufficient strength capacity to ensure that samples can be prepared for laboratory testing. The information of particular interest to the DGR setting relates the evolution of permeability during stress states that do not initiate failure in the rock to stress states that induce failure in the rock. Previous research conducted on the Cobourg Limestone indicated that *increases in the mean compressive stress* can lead to an *increase in the permeability*. The results of the present research confirm this finding by extending the studies to include deviatoric stress states. The exact processes that can contribute to the increase, which is quite unlike that observed in fine-grained

cylindrical samples can be viewed in relation to the stress states that induced failure. Figure 15 illustrates the post-failure values for the permeability determined at various stress states that induced failure of the Cobourg Limestone.

6 Discussion and Concluding Remarks

Cobourg Limestone is a heterogeneous nodular rock consisting of a calcite–dolomite nodular phase that is interspersed with a calcite–dolomite–quartz-rich argillaceous phase. The assessment of the fluid transport behavior of the rock is important because of its potential use as a site for a
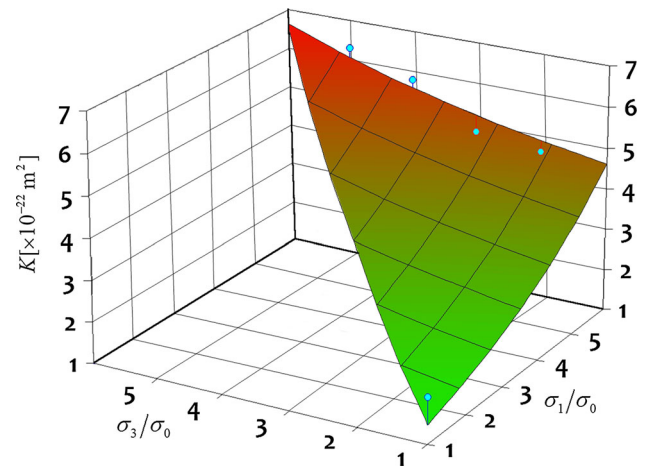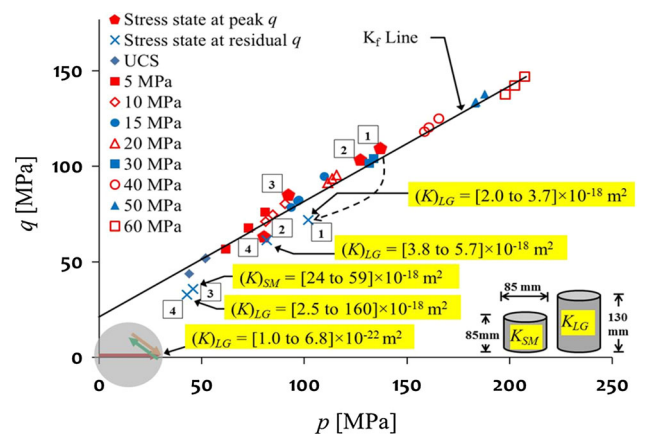
rocks such as limestone, sandstone and granite, where isotropic compression reduces the permeability, are most likely due to the development of heterogeneous stress states at the nodular fabric level of the rock, which can induce localized failure at the interfaces leading to permeability enhancement. The results of the experiments also show that the *permeability alterations are generally irreversible*. The results can, however, be used to develop a state-space permeability evolution relationship that depends on the maximum and minimum principal stresses. When stress states are below the failure threshold for the Cobourg Limestone, the permeability is within the range $K \in (1.0, 7.0) \times 10^{-22}$ m^2, which is consistent with results available in the literature. At these low ranges of permeabilities, it is likely that moisture migration within the rock can also be dictated by flow processes as well as diffusive phenomena. The combined flow-diffusive transport in low permeability can be examined in a theoretical context, but the development of experimental procedures that can detect moving boundaries between flow and diffusive regions is an area of research that has received limited attention. The interpretation of permeability of the Cobourg Limestone in terms of flow processes is, however, in keeping with previous research approaches and allows for comparisons.

The estimation of permeability of the Cobourg Limestone that has experienced failure is a non-routine exercise. The application of stress states that can induce failure needs to be matched with controlled experiments that can estimate the permeability either using steady-state tests or transient tests. An essential requirement for performing steady-state testing is that pathways exist for the flow of fluids through the fractured sample. In these investigations, it is found that the failure of the sample during triaxial stress states does create pathways that can be used to provide an estimate for the bulk permeability of the fractured rock in an axial direction. In the current experimental arrangements, there are no facilities for determining the dimensions of the evolving fractures and their orientations. As such, the permeability in the fractured state can only be interpreted in the sense of a bulk parameter. Also, the extension of the studies to include the estimation of permeabilities in the radial direction of the cylindrical sample requires a change in the experimental procedures. The axial flow steady-state permeability experiments performed indicate that the post-failure bulk permeability of the extensively fractured Cobourg Limestone varies in the range $K \in (2.0, 160) \times 10^{-18}$ m^2. It is also important to note that, disregarding the upper limit, the order of magnitude increase in the permeability for the larger Cobourg samples is around four orders. The bulk of the crack and failure development in the Cobourg Limestone occurred in

the argillaceous phase of the rock, and these phases were prone to defect development. Such a permeability increase in damaged zone has practical implications in establishing groundwater inflow rates in the vicinity of the underground repository during emplacement operations and the potential for radionuclide migration in the presence of a cross-repository hydraulic gradient. These evaluations can be established through computational simulations of the repository facility, hydromechanical couplings and by taking into consideration the geostatic stress states and permeability heterogeneity induced by the creation of the repository. To this end, NWMO in their *Geoscience Verification Plan* has developed procedures to collect in situ information to aid the verification of the extent of the EDZ and the EIZ. The methodologies proposed in this paper for the estimation of stress-induced permeability evolution will facilitate the estimation of stress-induced permeability alterations of the repository rocks and the influence of such impacts on the integrity and containment efficiency of the waste repository. The stress ranges over which the experiments were performed are relevant to deep geologic settings at depths of approximately 800 m, which is relevant to the envisaged repository siting depth. The scope of the research findings also has useful applications to the study fluid flow into base regions of slopes and open excavations that can contribute to rock slope failures induced by enhanced groundwater flow resulting from fracture and damage development. Finally, in the context of a deep geological waste repository setting and its long-term containment effectiveness, the phenomena most influencing radionuclide migration are the transport properties of the Excavation Damaged Zone (EDZ). This will involve issues related to permeability upscaling, mitigative construction methods, EDZ seals and their treatment in the context of a safety assessment. There is evidence to support the existence of diffusive transport in the Ordovician sequence, particularly in the Trenton Group of limestones and overlying shales. This is consistent with rock mass permeabilities of the order of 10^{-22} m^2, which are observed at the core scale ($\sim$ 0.1m), bore hole scale ($\sim$ 10 m) and formation scale ($\sim$1000 m).

References

Bear J (1972) Dynamics of fluids in porous media. American Elsevier, New York

Bernaix J (1969) New laboratory methods of studying the mechanical properties of rocks. Int J Rock Mech Min Sci 6:43–90

Biot MA (1941) General theory of three-dimensional consolidation. J Appl Phys 12:155–164

Brace WF, Walsh JB, Frangos WT (1968) Permeability of granite under high pressure. J Geophys Res 73:2225–2236

Brace WF (1978) A note on the permeability changes in geologic material due to stress. Pure Appl Geophys 116:627–633

Chapman NA, McKinley IG (1987) The geological disposal of nuclear waste. Wiley, New York

Cheng AH-D (2016) Poroelasticity. Springer, Berlin

Coussy O (2004) Poromechanics. Wiley, New York

David C, Wong T-F, Zhu W, Zhang J (1994) Laboratory measurement of compaction-induced permeability change in porous rocks: implications for the generation and maintenance of pore pressure excess in the crust. Pure Appl Geophys 143:425–456

Daw GP (1971) A modified Hoek–Franklin triaxial cell for rock permeability measurements. Geotechnique 21(89):91

Ding J (2013) Experimental study of rock deformation and permeability variation. MS Thesis, Texas A&M University

Fraser Harris AP, McDermott CI, Kolditz O, Haszeldine RS (2015) Modelling groundwater flow changes due to thermal effects of radioactive waste disposal at a hypothetical repository site near Sellafield, UK. Environ Earth Sci 74:1589–1602

Gartner Lee Ltd. (2008) Phase I geosynthesis. Report OPG 00216-REP-01300-000010-R00

Gleeson T, Ingebritsen S (eds) (2016) Crustal permeability. Wiley, New York

Gnirk P (1993) OECD/NEA International Stripa Project, Overview Volume II. Natural Barriers, Sweden: SKB: Stockholm

Golder Associates Ltd. (2003) LLW geotechnical feasibility study western waste management facility Bruce site Tiverton, Ontario. Report submitted to municipality of Kincardine and Ontario Power Generation. Report No. 021-1570

Gray MN (1993) OECD/NEA International Stripa Project Overview Volume III Engineered Barriers, Sweden: SKB: Stockholm

Gueguen Y, Bouteca M (2004) Mechanics of fluid-saturated rocks. International Geophysics Series, vol 89. Elsevier Academic Press

Han B, Xie SY, Shao JF (2016) Experimental investigation on mechanical behaviour and permeability evolution of a porous limestone under compression. Rock Mech Rock Eng. doi:10.1007/s00603-016-1000-6

Hart DJ, Wang HF (1998) Poroelastic effects during a laboratory transient pore pressure test. In: Thimus JF, Abousleiman Y, Cheng AH-D, Coussy O, Detournay E (eds) Poromechanics. A tribute to Maurice A. Biot, proceedings of the Biot conference in poromechanics, Louvain-la-Neuve. Balkema, Rotterdam, pp 579–582

Heystee R, Roegiers JC (1980) The effect of stress on primary permeability of rock cores-A facet of hydraulic fracturing. Can Geotech J 18:195–204

Hoek E, Franklin JA (1968) Simple triaxial cell for laboratory testing of rock. Trans Inst Min Metall 77:A22–A26

Hsieh PA, Tracy JV, Neuzil CE, Bredehoeft JD, Silliman SE (1981) A transient laboratory method for determining the hydraulic properties of 'tight' rocks—I. Theory. Int J Rock Mech Min Sci Geomech Abstr 18:245–252

Huertas F, Santiago JL, Fuentes-Cantillana JL, Farina P (2000) The FEBEX "in situ" test. Lessons learned, Euradwaste 1999 "Radioactive waste management strategies and issues". Fifth European commission conference on radioactive waste management and disposal and decommissioning, pp 353–357

INTERA (2011) Descriptive geosphere site model. Intera Engineering Ltd. Report for the Nuclear Waste Management Organization. NWMO DGR-TR-2011-24 R000: Toronto, Canada, 2011

Jensen M, Lam T, Luhowy D, McLay J, Semec B, Frizzell R (2009) Overview of Ontario power generation's proposed L&ILW geologic repository Bruce site, Tiverton, Ontario, ROCKENG09. In: Proceedings of the 3rd CANUS rock mechanics symposium, Toronto. Diederichs M, Grasselli G (eds) Paper 4253

Kiyama T, Kita H, Ishijima, Y, Yanagidani T, Akoi K, Sato T (1996) Permeability in anisotropic granite under hydrostatic compression and tri-axial compression including post-failure region. Proc 2nd North Amer Rock Mech Symp 1643–1650

Lanyon GW (2011) Excavation damaged zones assessment, NWMO DGR-TR 2011-21 prepared by Fracture Systems Ltd, pp 111

Laughton AS, Roberts LEJ, Wilkinson D, Gray DA (1986) The disposal of long-lived and highly radioactive wastes. In: Proceedings of a royal society discussion meeting, London: Royal Society

Liu ZB, Shao JF, Hu DW, Xie SY (2016) Gas permeability evolution with deformation and cracking processes in a white marble under compression. Transp Porous Media 111:441–455

Ma J, Wang J (2016) A stress-induced permeability evolution model for fissured porous media. Rock Mech Rock Eng 49:477–485

Massart TJ, Selvadurai APS (2012) Stress-induced permeability evolution in a quasi-brittle material. J Geophys Res. doi:10.1029/2012JB009251

Massart TJ, Selvadurai APS (2014) Computational analysis of dilatancy-induced permeability evolution in degrading geomaterials. Int J Rock Mech Min Sci 70:593–604

Mazurek M (2004) Long-term used nuclear fuel waste management-Geoscientific review of the sedimentary sequence in Southern Ontario. Technical Report TR 04-01: Institute of Geological Sciences, University of Bern, Bern, Switzerland

Muller TM, Sahay PN (2016) Generalized poroelasticity framework for micro-inhomogeneous rocks. Geophys Prospect 64:1122–1134

Neuzil CE (2012) Review: hydromechanical effects of continental glaciation on groundwater systems. Geofluids 12:22–37

Neuzil CE, Provost AM (2014) Ice sheet load cycling and fluid underpressures in the eastern Michigan Basin, Ontario, Canada. J Geophys Res. doi:10.1002/2014JB011643

Nguyen TS, Selvadurai APS (1998) A model for coupled mechanical and hydraulic behaviour of a rock joint. Int J Numer Anal Methods Geomech 22(1):29–48

Obert L (1963) An inexpensive triaxial apparatus for testing mine rock. Bureau of Mines Report of Investigations 6332, US Department of the Interior, Bureau of Mines

OECD (1988) Geological disposal of radioactive waste: in situ research and investigation in OECD countries. Paris, France: NEA Advisory Group, OECD

OPG (2011) Ontario power generation's deep geologic repository for low and intermediate level waste. Post-closure safety assessment: NWMO DGR-TR-2011-25

Pellet FL, Selvadurai APS (2016) Rock damage mechanics, chapter 3. In: Feng X-T (ed) Rock mechanics and engineering. CRC Press, Boca Raton, pp 65–108

Pusch R, Yong RN, Nakano M (2011) High level radioactive waste (HLW) disposal, a global challenge. Wessex Institute of Technology, Southampton

Raven K, Novakowski KS, Yager RM, Heystee RJ (1992) Supernormal fluid pressures in sedimentary rocks of southern Ontario: Western New York State. Can Geotech J 29:80–93

Rutqvist J, Chijimatsu M, Jing L, de Jonge J, Kohlmeier M, Millard A, Nguyen TS, Rejeb A, Souley M, Sugita Y, Tsang CF (2005)

Numerical study of the THM effects on the near-field safety of a hypothetical nuclear waste repository—BMT1 of the DECO-VALEX III project. Part 3: effects of THM coupling in fractured rock. Int J Rock Mech Min Sci 42:745–755

Schutjens PMTM, Heidug W (2012) On pore volume compressibility and its application as a petrophysical parameter. In: Biennial international conference and exposition on petroleum geophysics, Hyderabad, India, Paper SPG 011912

Selvadurai APS (1996a) Heat-induced moisture movement in a clay barrier. I Experimental modelling of borehole emplacement. Eng Geol 41:239–256

Selvadurai APS (1996b) Heat-induced moisture movement in a clay barrier. II Computational modelling and comparison with experimental results. Eng Geol 41:219–238

Selvadurai APS (2000) Partial differential equations in mechanics, vol. 1 Fundamentals, Laplace's Equation, The Diffusion Equation, The Wave Equation. Springer, Berlin

Selvadurai APS (2002) Influenced of pressurized water influx on the hygro–thermal behaviour of an engineered clay barrier in a waste emplacement borehole. Eng Geol 64:157–178

Selvadurai APS (2004) Stationary damage modelling of poroelastic contact. Int J Solids Struct 41:2043–2064

Selvadurai APS (2006) Gravity–driven advective transport during deep geological disposal of contaminants. Geophys Res Lett 33:L08408. doi:10.1029/2006GL025944

Selvadurai APS (2009) Influence of residual hydraulic gradients on decay curves for one-dimensional hydraulic pulse tests. Geophys J Int 177:1357–1365

Selvadurai APS (2015) Normal stress-induced permeability hysteresis of a fracture in a granite cylinder. Geofluids 15:37–47

Selvadurai APS (2017) Geomechanical characterization of the Cobourg Limestone. Technical Report submitted to the Nuclear Waste Management Organization, ON (In preparation)

Selvadurai APS, Carnaffan P (1997) A transient pressure pulse technique for the measurement of permeability of a cement grout. Can J Civ Eng 24:489–502

Selvadurai APS, Głowacki A (2008) Evolution of permeability hysteresis of Indiana Limestone during isotropic compression. Ground Water 46:113–119

Selvadurai APS, Ichikawa Y (2013) Some aspects of air-entrainment on decay rates in hydraulic pulse tests. Eng Geol 165:38–45

Selvadurai APS, Jenner L (2013) Radial flow permeability testing of an argillaceous limestone. Ground Water 51:100–107

Selvadurai APS, Najari M (2013) On the interpretation of hydraulic pulse tests on rock specimens. Adv Water Resour 53:139–149

Selvadurai APS, Najari M (2015) Laboratory-scale hydraulic pulse testing: influence of air fraction in the fluid-filled cavity in the estimation of permeability. Geotechnique 65:124–134

Selvadurai APS, Najari M (2016) Isothermal permeability of the argillaceous Cobourg Limestone. Oil Gas Sci Technol Rev IFP Energ Nouv 71:53–69

Selvadurai APS, Nguyen TS (1997) Scoping analyses of the coupled thermal-hydrological-mechanical behaviour of the rock mass around a nuclear fuel waste repository. Eng Geol 47(4):379–400

Selvadurai APS, Selvadurai PA (2010) Surface permeability test; experiments and modelling for estimating effective permeability. Proc R Soc Ser A Math Phys Sci 466:2819–2846

Selvadurai PA, Selvadurai APS (2014) On the effective permeability of a heterogeneous porous medium: the role of the geometric mean. Philos Mag 94:2318–2338

Selvadurai APS, Suvorov AP (2016) Thermo-poroelasticity and Geomechanics. Cambridge University Press, Cambridge

Selvadurai APS, Boulon MJ, Nguyen TS (2005) The permeability of an intact granite. Pure Appl Geophys 162:373–407

Selvadurai APS, Letendre A, Hekimi B (2011) Axial flow hydraulic pulse testing of an argillaceous limestone. Environ Earth Sci. doi:10.1007/s12665-011-1027-7

Shiping L, Yushou L, Yi L, Zhenye W, Gang Z (1994) Permeability–strain equations corresponding to the complete stress–strain path of Yinzhuang Sandstone. Int J Rock Mech Min Sci Geomech Abstr 31:383–391

Souley M, Homand F, Pepa S, Hoxha D (2001) Damage-induced permeability changes in granite: a case example at the URL in Canada. Int J Rock Mech Min Sci 38:297–310

Suvorov AP, Selvadurai APS (2010) Macroscopic constitutive equations of thermo-poroviscoelasticity derived using eigenstrains. J Mech Phys Solids 58:1461–1473

Sykes JF, Normani SD, Yin Y (2011) OPGs deep geologic repository for low and intermediate level waste. Hydrogeologic Modelling, NWMODGR-TR-2011-16

Tao T, Ghassemi A, Ehlig-Economides CA (2011) A fully coupled method to model fracture permeability change in naturally fractured reservoirs. Int J Rock Mech Min Sci 48:259–268

Tsang C-F, Birkholzer J, Rutqvist J (2008) A comparative review of hydrologic issues involved in geologic storage of CO_2 and injection disposal of liquid waste. Environ Geol 54(8):1723–1737. doi:10.1007/s00254-007-0949-6

Vilks P, Miller NH (2007) Evaluation of experimental protocols for characterizing diffusion in sedimentary rocks, Atomic Energy of Canada Limited. Nuclear Waste Management Division Report TR-2007-11. Toronto, Ontario

Wang HL, Xu WY, Shao JF (2014) Experimental researches on hydro-mechanical properties of altered rock under confining stress. Rock Mech Rock Eng 47:485–493

Wong LNY, Li D, Liu G (2013) Experimental studies on permeability studies on permeability of intact and singly jointed meta-sedimentary rocks under confining pressure. Rock Mech Rock Eng 46:107–121

Zhu W, Wong T-F (1997) The transition from brittle faulting to cataclastic flow: permeability evolution. J Geophys Res 102:3027–3041

Zoback MD, Byerlee JD (1975) The effect of microcrack dilatancy on the permeability of westerly granite. J Geophys Res 80:752–755